The 25th International Symposium on Automation and Robotics in Construction

June 26–29, 2008

ISARC-2008

Institute of Internet and Intelligent Technologies
Vilnius Gediminas Technical University
Saulėtekio al. 11, 10223 Vilnius, Lithuania
http://www.isarc2008.vgtu.lt/

EFFECT OF SCANNING DENSITY ON THE ACCURACY OF LOCATING SPHERE CENTERS FOR REGISTRATION

Marek Franaszek, Geraldine Cheok, Kamel Saidi, Christoph Witzgall
National Institute of Standards and Technology
100 Bureau Drive, Gaithersburg MD 20899, USA
marek@nist.gov, cheok@nist.gov, kamel.saidi@nist.gov, witzgall@ nist.gov

ABSTRACT

Applications for 3D imaging systems (e.g., laser scanners) have increased significantly in the past decade. Data from such systems often require registration. Spheres are often used for registration because they look the same from each direction and provide well defined reference points: fitted sphere centers. Common practice is to first scan individual targets at high density for high accuracy of fitted centers and then scan the entire scene at lower density. This, however, prevents the use of 3D imaging systems in a fully automated environment. It would thus be desirable to be able to determine the sphere centers from the low density scan. In this paper, we investigate how different scanning densities affect the locations of the fitted sphere centers. Analyses of high and low density scans show that high density scans are not necessary because the sphere centers can be estimated from sparse data without significant loss of accuracy.

KEYWORDS

3D imaging systems, target based registration, sphere fitting, construction automation

1. INTRODUCTION

Three-dimensional (3D) imaging systems are used for surveying, mapping and generation of 3D models [1]. 3D imaging systems are line-of-sight instruments and therefore parts of a scanned scene which are occluded from one scanner location have to be obtained from other locations to fill in the missing data. Since each scan is in the instrument's frame of reference, individual scans have to be registered to one common coordinate frame to provide a useful representation of the entire scanned object or scene.

Registration requires identification of at least three points common to all datasets to be registered. These common points may be selected by picking points from acquired dataset and in this case, the errors of their locations are a function of the instrument error and the ability to measure the exact same point from the two scans. Alternatively, fiduciary objects of known shape are placed in a scene to serve as easily identifiable targets. Then, the target centers can be derived by fitting known geometric primitives to the acquired points [2] which then can be used for registration. Errors in the locations of the fitted centers depend not only on the instrument error but

also on the fitting (e.g., a choice of error function). For nonlinear minimization, getting explicit values of errors may not be trivial.

Two types of targets are commonly used for registration: reflective planar targets and 3D targets. Spheres are especially convenient 3D targets compared to planar ones because their observed shapes do not change with varying viewpoints and therefore do not require re-orientation of the target. Spheres also allow registration of two datasets with little or no overlap and therefore, they give an operator more flexibility in choosing the scanner location.

At each scanner location, each sphere target is usually scanned individually at high density in order to minimize the error in locating the sphere center. The remaining scene is often scanned at a lower density to reduce the data acquisition time. This practice requires independent knowledge of target locations and manual intervention of an operator. This prevents the use of 3D imaging systems in a fully automated manner.

The elimination of the high-density scans would allow for automated processes and save time, thus, increasing productivity. This implies that fully automated procedures for finding sphere targets in large datasets, segmentation of the associated sphere points, and fitting of the spheres should be applied directly to low resolution scans. An important and practical question arises as to how reliably a sphere could be fitted to a sparse dataset.

In this paper, we study the effect of scanning density on estimating the fitted sphere center. Spheres were scanned at high density (thousands of data points per sphere) and low density (tens of data points per sphere) at varying distances. At each location of a sphere, its center was measured with higher accuracy using another type of instrument (total station or laser tracker). These more accurate measurements were used as ground truth for the sphere centers. In order to avoid adding the error caused by registration, data acquired in the scanner coordinate frame were not registered to the total station (or to the laser tracker) coordinate frame. Instead, the relative distance between a pair of fitted sphere centers was compared with the same distance obtained from the ground truth measurements. The difference between ground truth and fitted distance was used as a measure of the combined error (fitting error and instrument error). Due to the nonlinear minimization used for fitting, the error of the individual derived center was not evaluated.

2. EXPERIMENT

Two spheres made of different materials were used: one with radius R_{S1} = 76.2 mm and the other with R_{S2} = 50.8 mm. In actuality, Sphere S1 is not a sphere but a SMR (Spherically Mounted Retroreflector) (see Fig. 1). Sphere S1 was made of aluminum and then anodized. Sphere S2 was made of titanium and also anodized.

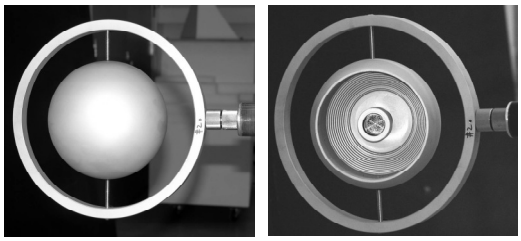

a) b)

Figure. 1 Sphere S1: a) front view; b) back view

Two scanners belonging to two different classes of 3D imaging systems were used. Instrument In1 has a manufacturer specified range error of approximately 7 mm (measured at a 100 m range) and maximum measurement range of 200 m. Instrument In2 has a maximum range of 24 m and a specified range error of 0.1 mm for ranges less than 10 m. For ranges between 10 m and 24 m, the range error is equal to 0.01 mm/m times range (in meters).

The data for this paper came from two experiments. In one experiment, Sphere S1 and Instrument In1 were used. In this experiment, the sphere was scanned in seven locations. The ground truth measurements were obtained using a total station with a manufacturer specified measurement error of ±0.2 mm. The experimental setup is shown in Fig. 2a. The datasets from this experiment will be called G1.

In the second experiment, both instruments, In1 and In2, were used to scan Sphere S2. The expanded

uncertainty of the ground truth measurements, obtained for this experiment with a laser tracker, was ±30 μm. For the combination of Instrument In1 and Sphere S2, the sphere was located in 14 locations, in the configuration shown in Fig. 2a. The datasets from this combination will be called G2. For the combination of Instrument In2 and Sphere S2, the sphere was located in 12 locations in the configuration shown in Fig. 2b. The datasets from this combination will be called G3.

In both experiments, the spheres were approximately collinear with each other and with the instrument.

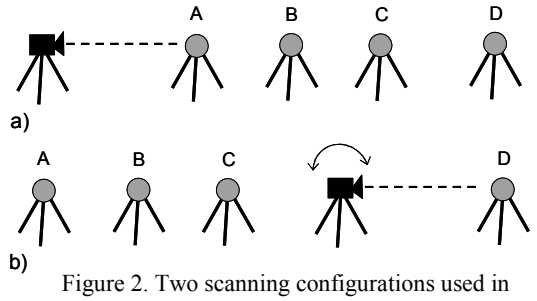

Figure 2. Two scanning configurations used in the experiments for datasets belonging to group: a) G1 and G2, b) G3

Every individual j-th dataset (j = A, B, C,…) was manually segmented and a sphere of known radius was fitted to the point cloud. Segmented datasets contained typically between 1200 and 4000 points for high density scans and between 6 and 40 points for low density scans. Fitting was done by the nonlinear Least Squares minimization of the generalized directional error function [3]. Then, the relative distance $F_H(k,j)$ between the two sphere centers $\boldsymbol{H}_k$ and $\boldsymbol{H}_j$ fitted to high density datasets k and j was calculated

$$F_H(k,j) = \left\| \boldsymbol{H}_k - \boldsymbol{H}_j \right\|, \tag{1}$$

where $k \neq j$ and ||…|| is the Euclidean norm. In a similar way, the relative distance $F_T(k,j)$ between two ground truth sphere locations, $\boldsymbol{T}_k$ and $\boldsymbol{T}_j$, (measured with the total station or laser tracker) was calculated (Fig. 3). Finally, the error $D_H(k,j)$ of the relative distances was calculated as

$$D_H(k,j) = F_H(k,j) - T(k,j). \tag{2}$$

The same procedure was repeated for the sparse datasets acquired with low density scans. Euclidean distance $F_L(k,j)$ between two fitted sphere centers $\boldsymbol{L}_k$ and $\boldsymbol{L}_j$ was calculated. The resulting error $D_L(k,j)$ was compared with $D_H(k,j)$, to determine the effect of scan density.

In addition, the difference $\Delta(j)$ of center $\boldsymbol{L}_j$ from $\boldsymbol{H}_j$ was calculated for every j-th sphere

$$\Delta(j) = \left\| \boldsymbol{H}_j - \boldsymbol{L}_j \right\| \tag{3}$$

Both errors, $D_H(k,j)$ for high density and $D_L(k,j)$ for low density scans, may assume either positive or negative values while $\Delta(j)$ is always greater than zero.

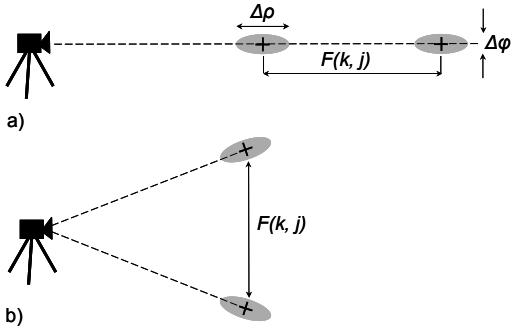

Figure 3. Two extreme scanning configurations: a) relative distance $F(k,j)$ between the two measured points has the largest possible variance; b) the smallest

In general, the main source of error in 3D imaging systems comes from the range measurement: both azimuth and elevation angle are determined with much smaller error. The error of a fitted sphere center (ρ, θ, φ) in spherical coordinates is expected to affect only range ρ, while errors in θ and φ are assumed to be negligible small. Elongated ellipsoidal error functions affect the error of fitted distances $F_L(k,j)$ and $F_H(k,j)$ differently in different experimental setups. In this context, the range datasets used for this project were collected in the worst case scenario: the scanner positions and consecutive sphere locations in every group G1-G3 were collinear. For such scanning configurations, the variance of the distance between two sphere centers, $var(F_H(k,j))$, is the largest possible and equal to

$var(\rho_j)$ + $var(\rho_k)$, see Fig. 3a. For any other configuration, including the extreme one shown in Fig. 3b, geometry constraints will cause partial cancellation of variances $var(\rho_j)$ and $var(\rho_k)$.

3. RESULTS

Fig. 4 shows the difference between the two sphere centers, $\Delta(j)$, fitted to the low and high density scans for the seven pairs of datasets belonging to group G1. The sphere locations are labeled A through G and the distance, $d(j)$, from each sphere center to the scanner is also given on the horizontal axis. The distance $d(j)$ was set equal to the average of the two distances

$$d(j) = (\| \boldsymbol{H}_j \| + \| \boldsymbol{L}_j \|)/2 \ . \qquad (4)$$

As we mentioned earlier, the uncertainty of the fitted sphere center could not be evaluated at this time and therefore we are unable to provide uncertainty for the difference $\Delta(j)$. For reference, the dashed line in Fig. 4 represents the lower bound of the uncertainty for the relative distance between two measured points, Ω, which is equal to the $\sqrt{2}$ times the instrument error. This is a lower bound because Ω consists only of the instrument error. For instrument In1, it is equal to 9.9 mm.

In Fig. 5, the errors of the relative distances for all possible pairs (k,j) of fitted sphere centers selected from G1 are shown. The data in the upper triangle (above the black diagonal line, $k > j$) correspond to $D_H(k,j)$ for high density scans while data below the diagonal ($k < j$) correspond to $D_L(k,j)$ for low density scans. Data on diagonal is filled with zeros for reference. Fig. 6 shows $\Delta(j)$ for the 14 pairs of datasets constituting G2. Dashed line corresponds to the same lower bound of error as in Fig. 4.

Fig. 7 displays $D_H(k,j)$ (above the diagonal line) and $D_L(k,j)$ (below the diagonal line) for G2. Again, points on the diagonal were assigned zero values for reference. The dashed line corresponds to the same lower bound of error as in Fig. 4. Fig. 7 displays $D_H(k,j)$ (above the diagonal line) and $D_L(k,j)$ (below the diagonal line) for G2. Again, points on the diagonal were assigned zero values for reference.

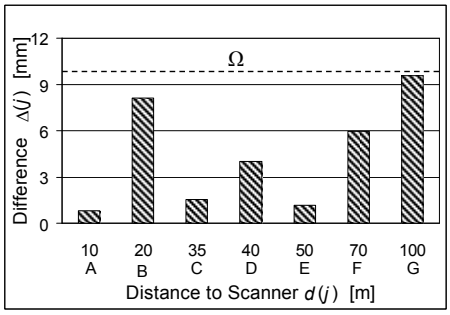

Figure 4. Difference $\Delta(j)$ vs. distance $d(j)$ for datasets in group G1

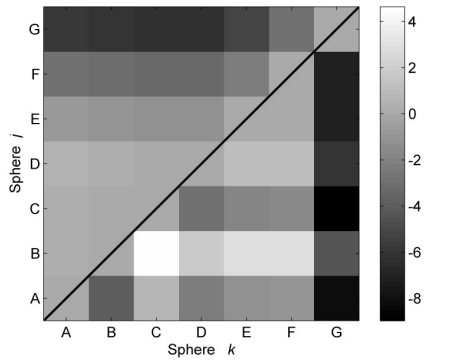

Figure 5. Errors, $D_H(k,j)$ and $D_L(k,j)$, for group G1: high density above diagonal and low density below diagonal, varying between -8 mm and +4 mm

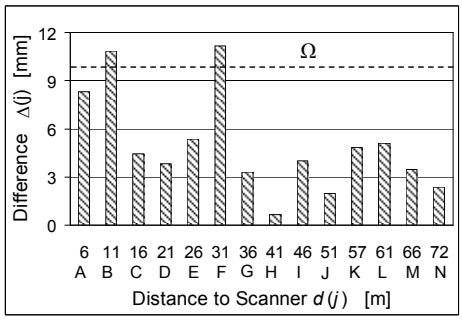

Figure 6. Difference $\Delta(j)$ vs. distance $d(j)$ for datasets in group G2

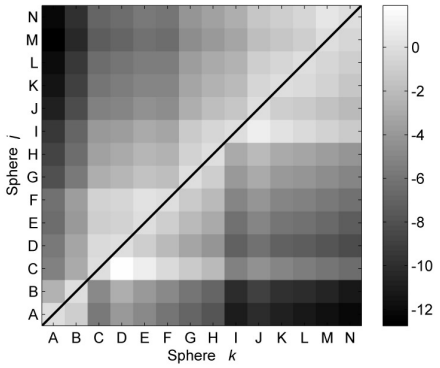

Figure 7. Errors, $D_H(k,j)$ and $D_L(k,j)$, for group G2: high density above diagonal and low density below diagonal, varying between -12 mm and +2 mm

Fig. 8 presents difference $\Delta(j)$ for group G3. Datasets in this group were acquired in the configuration shown in Fig. 2b. While the scanner position remained fixed, the scanning direction for datasets A, B and C was flipped by 180º to the scanning direction for the rest of datasets in this group. Therefore, the distance $d(j)$ defined by (4) is now negative for j = A, B and C. The lower bound of the error for the relative distance for instrument In2 is 0.14 mm ($\sqrt{2}$ x 0.1 mm).

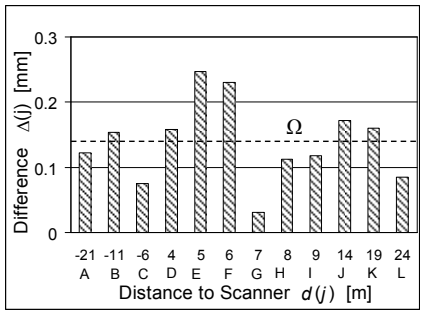

Figure 8. Difference $\Delta(j)$ vs. signed distance $d(j)$ for datasets in group G3

Fig. 9 shows the errors $D_H(k,j)$ (above the white diagonal line) and $D_L(k,j)$ (below the diagonal line) for G3. Again, points on the diagonal were assigned zero value for reference.

The data shown in Fig. 7 as the first column $D_H(\mathrm{A}, n)$ and the first row $D_L(n, \mathrm{A})$ are reproduced in Fig. 10 where the values are plotted against the distances between the true sphere center A and the remaining true centers n = B, C, …, N. Similarly, the data from Fig. 9 are redrawn in Fig. 11, i.e. errors $D_H(\mathrm{A}, n)$ and $D_L(n, \mathrm{A})$ against the distances between the true sphere center A and the remaining true centers n = B, C, …, L.

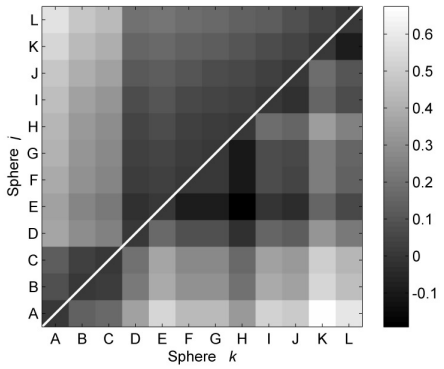

Figure 9. Errors, $D_H(k,j)$ and $D_L(k,j)$, for group G3: high density above diagonal and low density below diagonal, varying between -0.1 mm and +0.6 mm

4. DISCUSSION AND CONCLUSIONS

For all three groups G1-G3, the differences $\Delta(j)$ as well as the errors D_H and D_L are comparable to the error of relative distance between two data points acquired with the given 3D imaging instrument. This means that using the derived sphere centers as points for registration is at least as good as the selection of individual points from the datasets. We expect that the uncertainty associated with the former method to be less than the latter method which includes instrument error and the ability to select the exact same points in two datasets. However, this requires further study into determining the uncertainty of the fitted center. For most pairs (k,j), the error D_H calculated for the high density data set is only slightly less than the corresponding D_L for the low density data (see Figs. 10 and 11). In fact, for about a third of all pairs D_H is larger than D_L (33 % of pairs for G1, 41 % for G2 and 35 % for G3). Thus, in most cases, the scanning density had little impact on the location of derived sphere centers. Figs. 5, 7 and 9 also reveal a well defined pattern for the dense and

sparse datasets: generally, the larger the distance between sphere centers, the larger the errors D_H and D_L are (Figs. 10 and 11). As expected, the errors D_H and D_L increase as the distance between sphere centers increases because the range error typically increases with distance. The variations of $\Delta(j)$ do not follow this same pattern and we do not understand why this is so. This will require further investigation.

The data shown in Figs. 5 and 7 reveal that most of errors have negative values while most of the data in Fig. 9 have positive values. One may expect that differences from ground truth should be random, i.e., both positive and negative signs should be equally frequent.

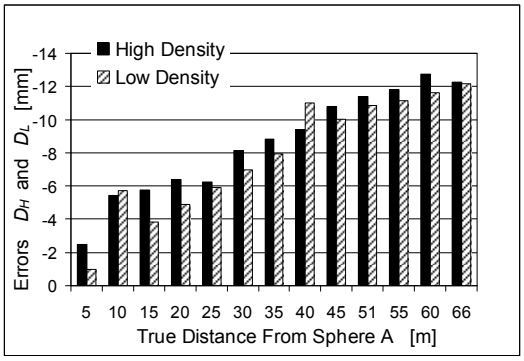

Figure 10. Errors D_H(A, n) and D_L(n, A) for G2

Negative D_H defined by (2) means that the distance $F_H(k,j)$ between the pair of spheres is systematically underestimated, which leads to the conclusion that the corresponding fitted sphere centers yield underestimated ranges $\|\boldsymbol{H}_k\|$ and $\|\boldsymbol{H}_j\|$ (the same is true for D_L and $\|\boldsymbol{L}_k\|$, $\|\boldsymbol{L}_j\|$). For the data shown in Fig. 9, the opposite trend is evident: D_H and D_L are mostly positive which indicates that the fitted sphere centers yield overestimated ranges $\|\boldsymbol{H}_k\|$ and $\|\boldsymbol{H}_j\|$ (and the same is true for $\|\boldsymbol{L}_k\|$ and $\|\boldsymbol{L}_j\|$). One explanation of this effect is that the instrument systematically under- or over- estimates the range due to offsets within the instrument itself. All datasets in group G1 and G2 were acquired with instrument In1 while all datasets in G3 were collected with In2.

While the errors $D_L(k,j)$ and $D_H(k,j)$ give a direct indication of how the derived distances $F_L(k,j)$ and $F_H(k,j)$ differ from ground truth, the difference $\Delta(j)$ is not related to ground truth. Instead, it quantifies the sensitivity of the fitted sphere center to variations in the dataset.

Keeping in mind the large difference in the number of points between the dense and sparse datasets (more than two orders of magnitude), the differences $\Delta(j)$ shown in Figs. 4, 6 and 8 reveal a robustness of sphere fitting procedure.

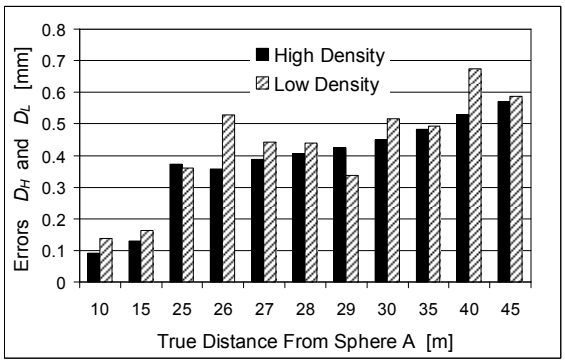

Figure 11. Errors D_H(A, n) and D_L(n, A) for G3.

In summary, the presented data support the conclusion that, in most cases, the scanning density had little impact on the determination of the derived sphere centers. Thus, high density scanning of sphere targets may not be necessary. The elimination of this step will increase the efficiency of the scanning process. The results indicate that the centers of the spheres fitted to the sparse data can be determined without significant loss of accuracy as compared to the centers obtained from fitting high density data.

REFERENCES

[1] Stone W.C., Juberts M., Dagalakis N., Stone J. & Gorman J. (2004) Performance Analysis of Next-Generation LADAR for Manufacturing, Construction, and Mobility, *NISTIR 7117*.

[2] Gander W., Golub G.H. & Strebel R. (1994) Least-squares fitting of circles and ellipses, *BIT*, Vol. 34, pp. 558–578.

[3] Witzgall C., Cheok G.S. & Kearsley A.J. (2006) Recovering Circles and Spheres from Point Data, in *Perspectives in Operations Research*, Springer, pp. 393–413.